Supplementary Information (SI) for ChemComm.
This journal is © The Royal Society of Chemistry 2025

Supporting Information

for

Controllable properties of NiO nanostructures fabricated by plasma assisted-chemical vapor deposition

Table of Contents

§ S1. Experimental

§ S1-1. Synthesis

Plasma assisted-chemical vapor deposition (PA-CVD) of NiO was performed starting from the $Ni(tfa)_2$•TMEDA precursor (Htfa = 1,1,1-trifluoro-2,4-pentanedione; TMEDA = *N*,*N*,*N'*,*N'*-tetramethylethylenediamine], previously synthesized and characterized,[1, 2] on pre-cleaned[3] fluorine-doped tin oxide (FTO)-coated glass substrates (Aldrich®; ≈7 $\Omega\times sq^{-1}$; FTO thickness ≈600 nm). The latter were fixed with metallic clips on the grounded electrode of a custom-built two-electrode radio frequency (RF, ν = 13.56 MHz) plasmochemical reactor,[4] whereas RF-power was delivered to the second electrode (electrode-to-electrode distance = 6.0 cm). Basing on preliminary optimization experiments, syntheses were carried out from electronic grade Ar/O_2 plasmas [flow rates = 15 and 5 standard cubic centimeters per minute (sccm), respectively], using a total pressure of 1.0 mbar and a RF-power of 20 W. The used growth temperature was 100°C, and the process duration was set at 10 min, 30 min, 60 min, and 90 min, respectively. $Ni(tfa)_2$•TMEDA powders (0.15 g for each deposition), introduced in an external glass reservoir, were heated at 75°C by means of an external oil bath and their vapors were transported into the reactor by an additional Ar flow (rate = 60 sccm) through heated gas lines. After deposition, the samples were annealed at 600°C (heating rate = 10 °C/min) for 1 h in air.

§ S1-2. Chemico-physical characterization

X-ray diffraction (XRD) measurements were carried out by using a Panalytical Empyrean diffractometer, operating in Bragg-Brentano (BB) mode, using a Cu Kα X-ray source (λ=1.54056 Å) powered at 40 kV and 40 mA. The instrument is equipped with a Pix-Cel two-dimensional detector for BB acquisitions with a 255×255 array sensor, covering a 3°×3° solid angle. The texture coefficients (TC_{hkl}) were calculated as:[5, 6]

$$TC_{hkl} = (I_{hkl}/I^0_{hkl}) \,/\, \{(1/N)*[\Sigma(I_{hkl}/I^0_{hkl})]\} \qquad (S1)$$

where I_{hkl} and I^0_{hkl} are the diffracted intensities corresponding to the (hkl) planes for the analysed sample and the reference NiO pattern, respectively,[7] and N is the overall number of reflections observed in the specimen XRD pattern.

X-ray photoelectron spectroscopy (XPS), ultraviolet photoelectron spectroscopy (UPS), and reflection electron energy loss spectroscopy (REELS) analyses were performed through a ThermoFisher ESCALAB QXi apparatus, funded by “Sviluppo delle infrastrutture e programma biennale degli interventi del Consiglio Nazionale delle Ricerche (2019)”, equipped with a monochromatized Al Kα X-ray source (hν = 1486.6 eV). Binding energy (BE) values were corrected for charging by referencing the adventitious C1s signal [component (a) in Fig. S4] at 284.8 eV. Atomic percentages (at.%) were computed by peak area integration, using ThermoFisher sensitivity factors. Peak fitting was carried out by XPSpeak software,[8] using Gaussian-Lorentzian sum functions and applying a Shirley-type background subtraction. Ar^+ sputtering was carried out at 4.0 kV (Ar partial pressure = 5×10^{-8} mbar). UPS analysis was carried out using a He(I) ($h\nu = 21.22$ eV) photon source generated by a helium plasma lamp. Work function measurements were carried out with the sample biased at −3.0 V.[9] REELS analysis was performed using a primary beam energy of 1.0 keV.

Atomic force microscopy (AFM) characterization was performed in air using an NT-MDT SPM Solver P47H-PRO instrument operated in tapping mode. Micrographs recorded on different specimens areas enabled to ascertain surface homogeneity. After background subtraction and plane fitting, root-mean-square (RMS) roughness values were obtained as previously reported.[10]

Field emission-scanning electron microscopy (FE-SEM) analyses were performed using a Zeiss SUPRA 40 VP instrument, at primary beam acceleration voltages of 10-20 kV. The average deposit thickness, as well as the mean grain and island sizes and distribution of length of void spaces (see Fig. S10), were obtained by a statistical image analysis, using the ImageJ® software (version 1.54 k).[11]

Optical transmission spectra of NiO thin films were collected on Agilent Cary 60 instrument, at normal incidence and in air.

§ S1-3. Wetting properties and photodegradation performances

Wettability of NiO deposits was studied by means of water contact angle (WCA) measurements. Three separate drops of distilled water (3.0 μL) were dripped onto each sample, recorded and analysed with an Attension Theta Light goniometer from Biolin Scientific. The WCA was determined using the Young equation.[12] The samples were air dried and put into an air-cooled top-down illumination box, equipped with UVA lamps ($\lambda_{max} = 365$ nm, see also Fig. S11) with intensity of 3606.5 μW/cm^2 for the set time period.

For solid-phase photocatalytic oxidation tests, the samples were dip-coated with a 0.2 M solution of methyl stearate in *n*-hexane at a withdrawal speed of 10 cm/min, and subsequently air-dried. This process produced a uniform coating of the fatty compound on the sample surface.[13] Subsequently, WCA measurements were carried out as for the pristine specimens. The same illumination setup was used for photocatalytic degradation of diclofenac (DCF) with the addition of a petri dish (D=80 mm, H=45 mm), a magnet and an off-centre placed thin film sample. The concentration of diclofenac was 1 mg/L, and the reaction volume was 40 mL with the native pH. DCF concentration was determined by high performance liquid chromatography (HPLC) on an Agilent 1260 Infinity II chromatograph using a C-18 column Poroshell 120, 4.6 × 50 mm^2 with a flow of 0.7 mL/min. The solvent composition was 0.1% acetic acid (50%): acetonitrile (50%) in isocratic mode. The injection volume was 20 μL.

§ S2. Additional characterization results

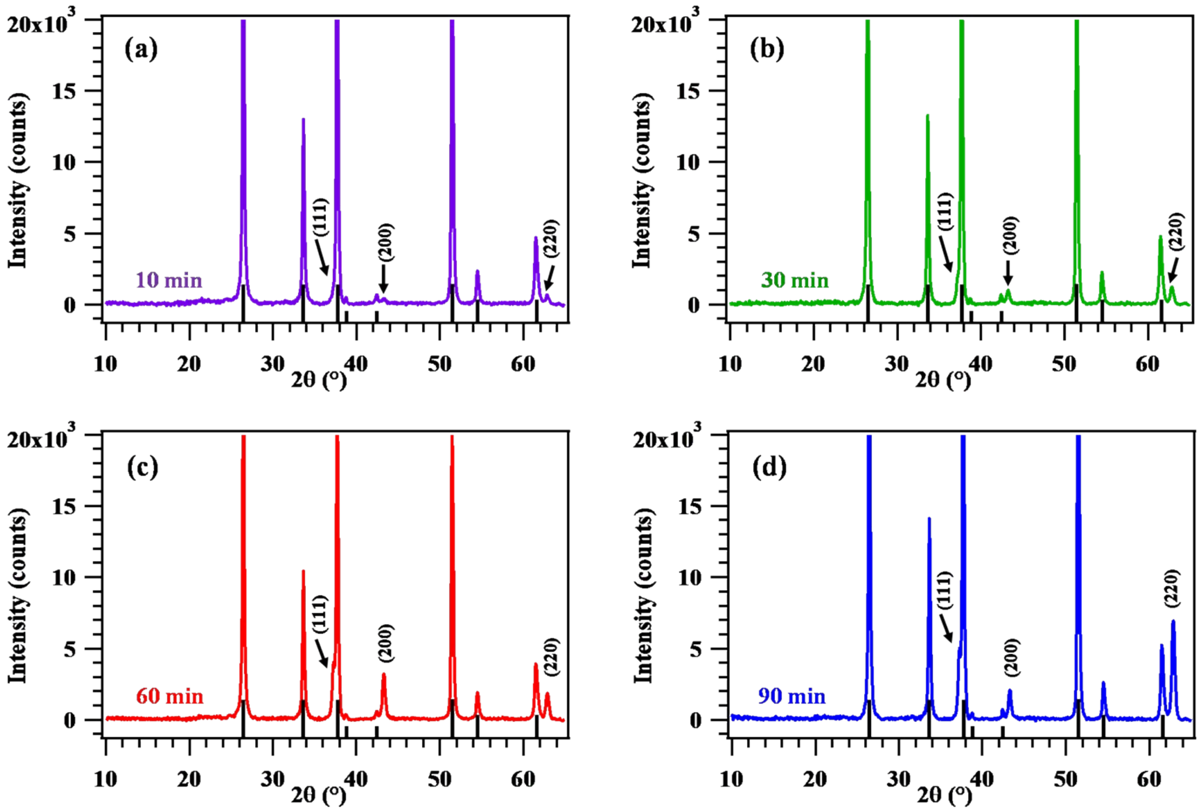

Fig. S1 XRD patterns of NiO samples obtained at different deposition times. Vertical black bars mark FTO substrate reflections.

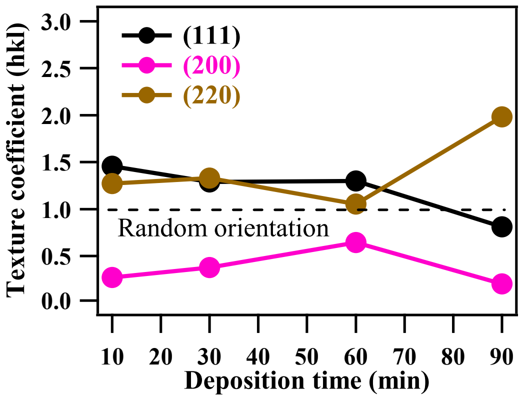

Fig. S2 Texture coefficients (TC) calculated for the (111), (200), and (220) planes for NiO specimens obtained at different deposition times. The obtained TC values evidence the preferential growth along [111] and [220] directions, the latter becoming predominant for a deposition time of 90 min.[5, 14]

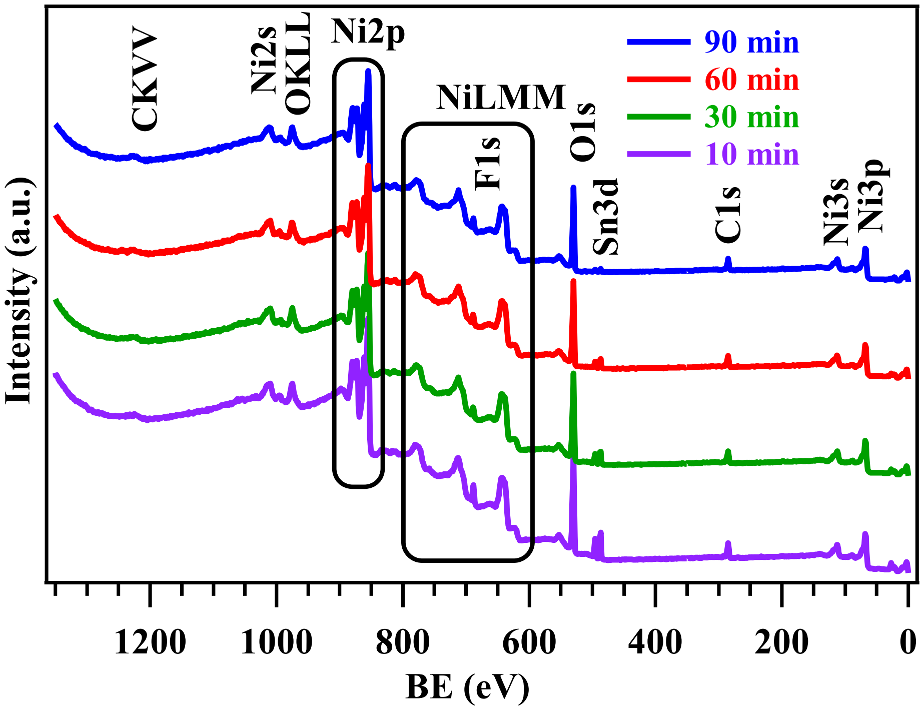

Fig. S3 XPS wide-scan spectra for the NiO samples investigated in the present work.

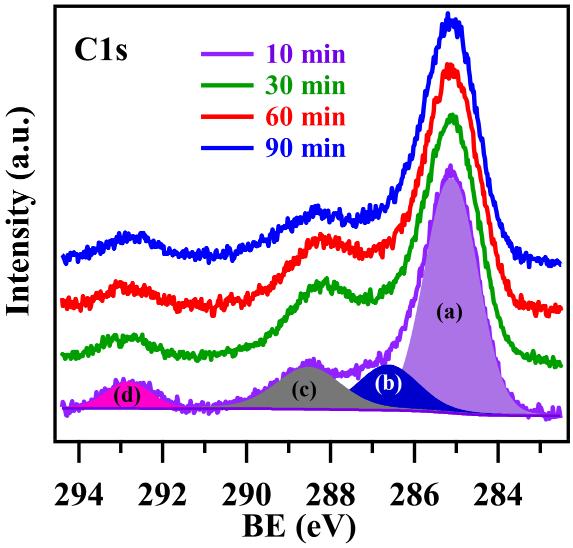

Fig. S4 C1s photoelectron peaks for NiO specimens obtained at different deposition times.

sample	(a)		(b)		(c)		(d)	
	BE (eV)	%	BE (eV)	%	BE (eV)	%	BE (eV)	%
10 min	284.8	63.4	286.3	12.9	288.2	16.3	292.5	7.4
30 min	284.8	60.1	286.3	13.6	288.0	21.5	292.5	4.8
60 min	284.8	59.9	286.3	12.8	288.0	21.7	292.6	5.6
90 min	284.8	66.2	286.3	10.3	288.1	16.9	292.5	6.6

Table S1 BEs and % contributions of the various bands with respect to the overall C1s photopeak for the various NiO samples. Color codes of components (a), (b), (c), and (d) as in Fig. S4.

The C1s signal (Fig. S4) could be fitted by means of four distinct components (Table S1). Bands (a) and (b), located at BE = 284.8 eV and 286.3 eV, respectively, were attributed to adventitious carbon contamination and to surface C-O moieties.[13, 15, 16] The two components located at ≈288.1 eV (c) and ≈292.5 eV (d) were respectively ascribed to chemisorbed carbonates[17, 18] and to CF_x residuals from the used Ni precursor.[13, 19]

For all samples, XPS analyses revealed the presence of fluorine (Fig. S5; peak at 688.2 eV), due to CF_x groups from the precursor.[13, 19] This signal could be reduced to noise level after Ar^+ erosion for 5 min.

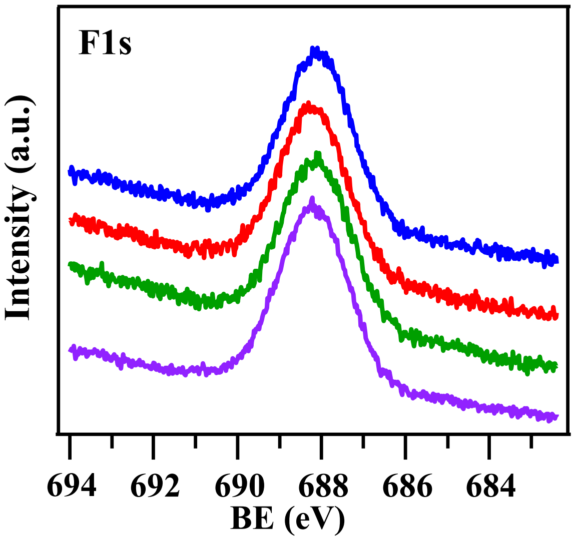

Fig. S5 F1s photoelectron peaks for NiO specimens obtained at different deposition times.

Sample	(I)		(II)	
	BE (eV)	%	BE (eV)	%
10 min	529.9	61.2	531.5	38.8
30 min	529.9	57.2	531.5	42.7
60 min	529.8	58.4	531.5	41.6
90 min	529.9	64.2	531.5	35.8

Table S2 BEs and % contributions of the various bands with respect to the overall O1s photopeak for the various NiO samples. Color codes of components (I) and (II) as in Fig. 1c.

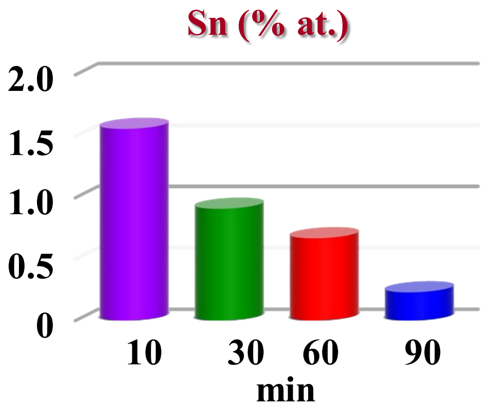

Fig. S6 Sn atomic percentage (at.%) as a function of deposition time for the analyzed NiO samples.

sample	**IP (eV)**	**EA (eV)**	**E_G (eV)**	**E_F – VB (eV)**
10 min	5.3	1.7	3.6	0.57
30 min	5.3	1.8	3.4	0.55
60 min	5.2	1.8	3.4	0.52
90 min	5.2	1.8	3.3	0.48

Table S3 Ionization potential (IP), electron affinity (EA), energy gap values (E_G, estimated by REELS), and valence band edge separation from the Fermi level (E_F − VB) for the various NiO specimens. W_F corresponds to $E_F - E_{vacuum}$, whereas IP (EA) are evaluated as the difference between the valence (conduction) band edges (VB and CB, respectively) and the vacuum level energy.[9]

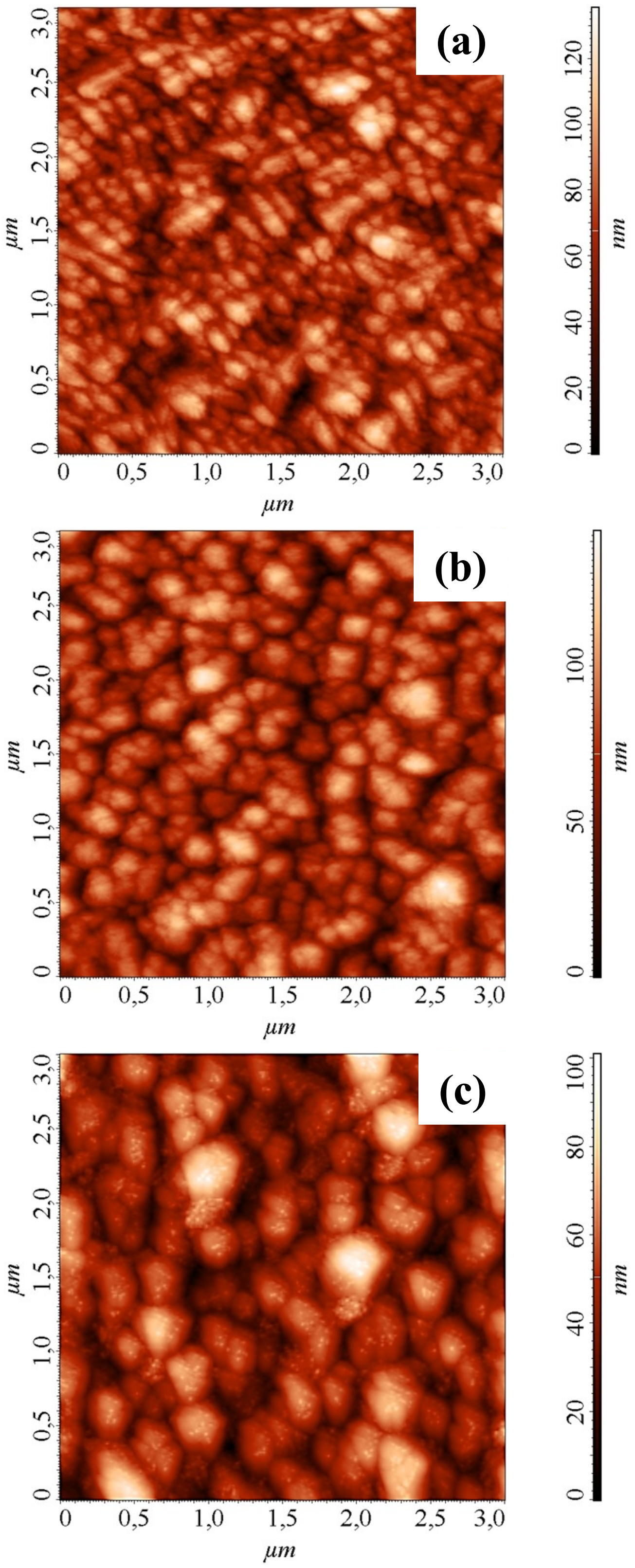

Fig. S7 AFM micrographs for NiO specimens obtained at deposition times of 30 min (a), 60 min (b), and 90 min (c). The RMS roughness values are all very close to 16 nm.

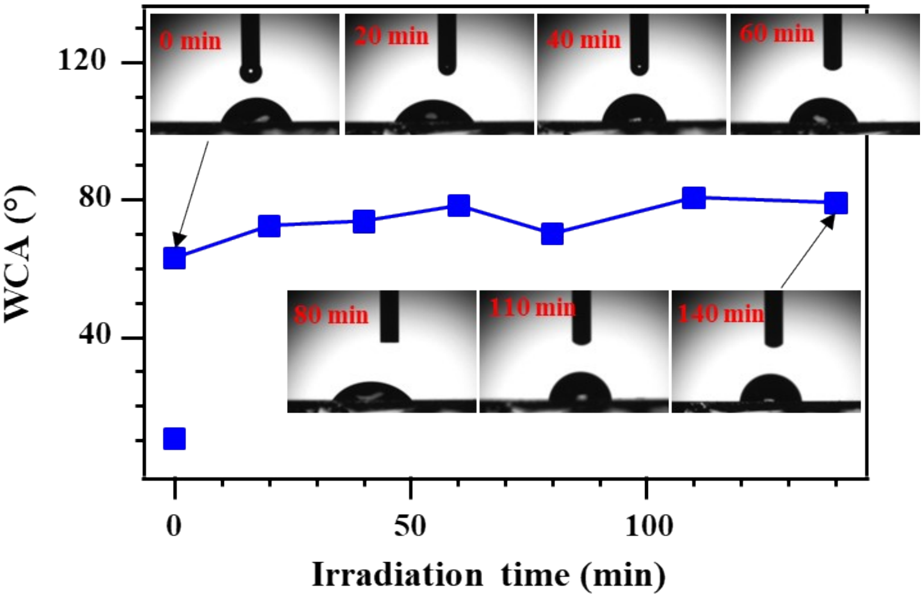

Fig. S8 Temporal evolution of water droplets on a NiO specimen obtained for a process duration of 90 min at different illumination stages. Note that the photographs show a snapshot of a particular droplet, whereas the values of the experimental points represent an average of three droplets taken at three different locations on the same sample.

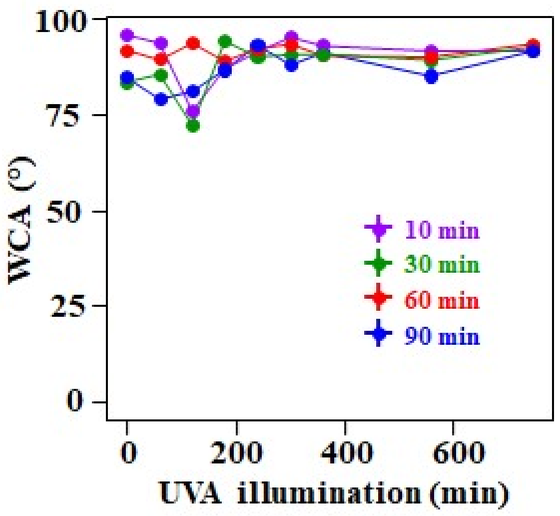

Fig. S9 Changes in water contact angle during UVA illumination of the different NiO films covered with a methyl stearate layer.

sample	***k* (min^{-1})**
10 min	0.49×10^{-3}
30 min	0.72×10^{-3}
60 min	1.02×10^{-3}
90 min	1.46×10^{-3}

Table S4 Values of the apparent kinetic constants (*k*) concerning DCF degradation for NiO specimens obtained at different deposition times.

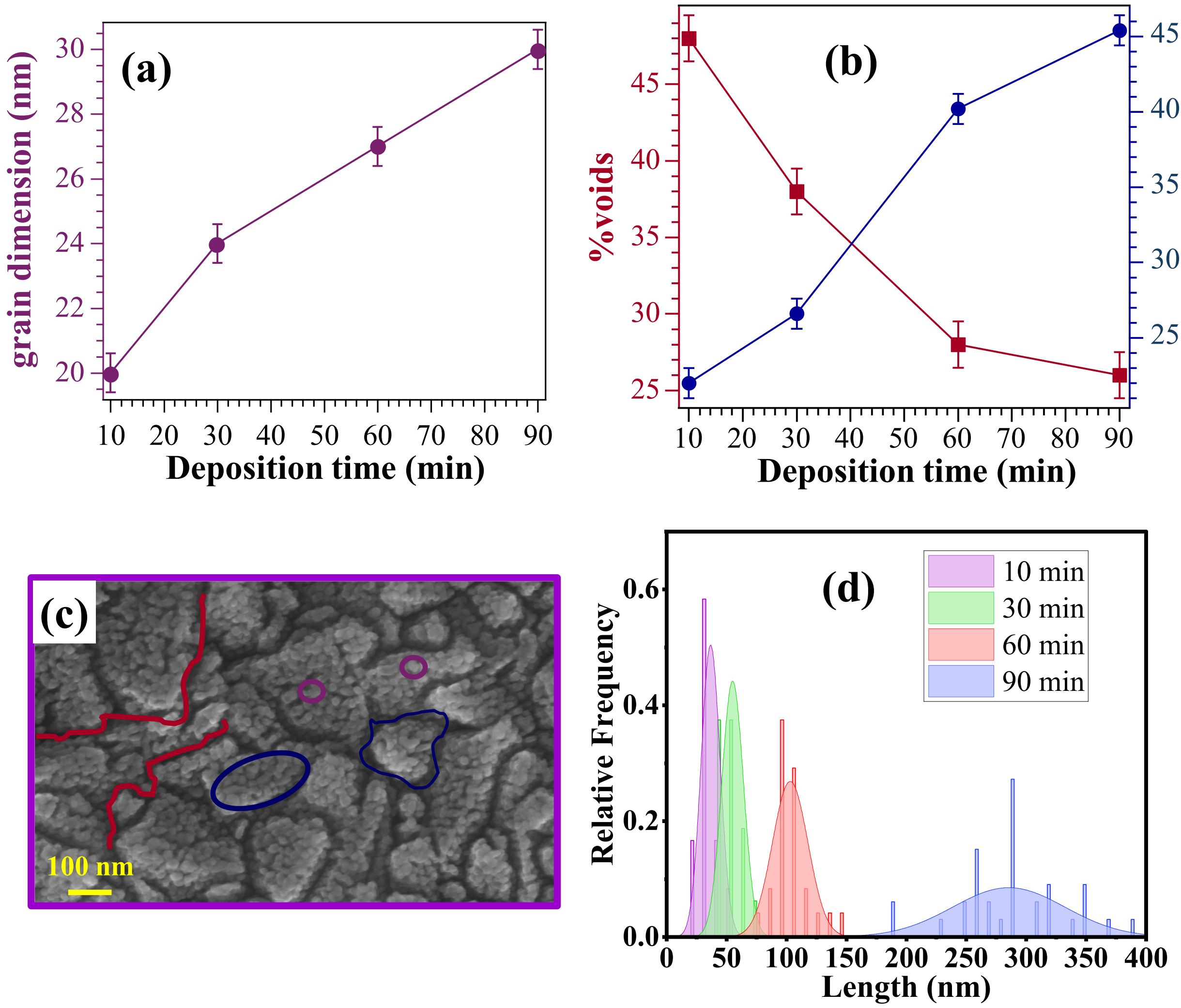

Fig. S10 (a) Grain dimensions and (b) % of voids and mean island sizes for the target NiO specimens as a function of the adopted deposition time. Color codes as in the FE-SEM image (c), pertaining to a NiO sample obtained with a process duration of 90 min. (d) Distribution of length of void spaces between NiO columns. The data were obtained by elaboration of FE-SEM micrographs.

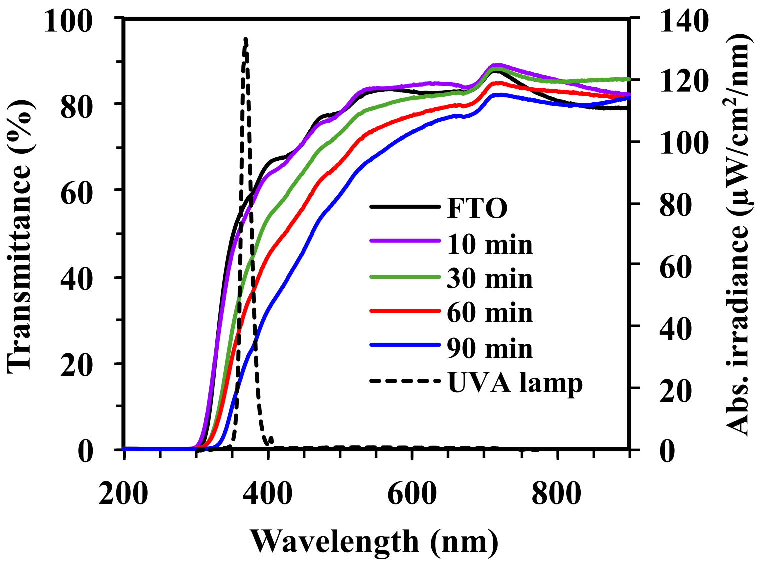

Fig. S11 Front-face optical transmittance spectra of NiO specimens recorded after DCF degradation (left vertical axis), and emission spectrum of the low-pressure UVA lamp (right vertical axis). Before spectra collection, all the systems were carefully washed with deionized water.

§ S3. References

1 M. Benedet, D. Barreca, E. Fois, R. Seraglia, G. Tabacchi, M. Roverso, G. Pagot, C. Invernizzi, A. Gasparotto, A. A. Heidecker, A. Pöthig, E. Callone, S. Dirè, S. Bogialli, V. Di Noto and C. Maccato, *Dalton Trans.*, 2023, **52**, 10677–10688.

2 C. Invernizzi, G. Tabacchi, R. Seraglia, M. Benedet, M. Roverso, C. Maccato, S. Bogialli, D. Barreca and E. Fois, *Molecules*, 2024, **29**, 642.

3 D. Barreca, G. Carraro, A. Gasparotto, C. Maccato, C. Sada, A. P. Singh, S. Mathur, A. Mettenbörger, E. Bontempi and L. E. Depero, *Int. J. Hydrogen Energy*, 2013, **38**, 14189-14199.

4 D. Barreca, A. Gasparotto, E. Tondello, C. Sada, S. Polizzi and A. Benedetti, *Chem. Vap. Deposition*, 2003, **9**, 199-206.

5 S. K. Kuanr, G. Vinothkumar and K. S. Babu, *Mater. Sci. Semicond. Process.*, 2018, **75**, 26-30.

6 L. Bigiani, D. Barreca, A. Gasparotto, C. Sada, S. Martí-Sanchez, J. Arbiol and C. Maccato, *CrystEngComm*, 2018, **20**, 3016-3024.

7 Pattern n°00-0047-1049, JCPDS, 2000.

8 https://xpspeak.software.informer.com/4.1/; Accessed October, 2024.

9 M. Benedet, C. Maccato, G. Pagot, C. Invernizzi, C. Sada, V. Di Noto, G. A. Rizzi, E. Fois, G. Tabacchi and D. Barreca, *J. Phys. Chem. C*, 2023, **127**, 22304-22314.

10 M. Benedet, G. A. Rizzi, A. Gasparotto, O. I. Lebedev, L. Girardi, C. Maccato and D. Barreca, *Chem. Eng. J.*, 2022, **448**, 137645.

11 https://imagej.net/ij/; Accessed September, 2024.

12 H. Jiang, F. Müller-Plathe and A. Z. Panagiotopoulos, *J. Chem. Phys.*, 2017, **147**, 084708.

13 D. Barreca, F. Gri, A. Gasparotto, G. Carraro, L. Bigiani, T. Altantzis, B. Žener, U. Lavrenčič Štangar, B. Alessi, D. B. Padmanaban, D. Mariotti and C. Maccato, *Nanoscale*, 2019, **11**, 98-108.

14 L. Znaidi, T. Touam, D. Vrel, N. Souded, S. Ben Yahia, O. Brinza, A. Fischer and A. Boudrioua, *Coatings*, 2013, **3**, 126-139.

15 D. Briggs and M. P. Seah, *Practical Surface Analysis: Auger and X-ray Photoelectron Spectroscopy*, John Wiley & Sons: New York, 2nd ed., 1990.

16 J. F. Moulder, W. F. Stickle, P. E. Sobol and K. D. Bomben, *Handbook of X-ray Photoelectron Spectroscopy*, Perkin Elmer Corporation, Eden Prairie, MN, USA, 1992.

17 G. Pagot, M. Benedet, C. Maccato, D. Barreca and V. Di Noto, *Surf. Sci. Spectra*, 2023, **30**, 024028.

18 N. Weidler, J. Schuch, F. Knaus, P. Stenner, S. Hoch, A. Maljusch, R. Schäfer, B. Kaiser and W. Jaegermann, *J. Phys. Chem. C*, 2017, **121**, 6455-6463.

19 G. Carraro, A. Gasparotto, C. Maccato and D. Barreca, *Surf. Sci. Spectra*, 2013, **20**, 9-16.